
Article:
Li, Z. and Long, H. (2026) Developing a new wrinkling testing method for sheet metal spinning. The International Journal of Advanced Manufacturing Technology. ISSN: 0268-3768

https://doi.org/10.1007/s00170-026-17740-3

The International Journal of Advanced Manufacturing Technology
https://doi.org/10.1007/s00170-026-17740-3

ORIGINAL ARTICLE

Developing a new wrinkling testing method for sheet metal spinning

Zhikun Li[1] · **Hui Long**[1]

Received: 13 September 2025 / Accepted: 11 February 2026

Abstract

Wrinkling is a common process failure in spinning; there are no established testing methods to obtain strain limits to predict and prevent wrinkling. Mechanisms of wrinkling initiation and growth as well as associated strain conditions and their limits are unclear. This study firstly investigates strain variations under different process conditions by developing finite element (FE) simulation and experiment of a shear spinning process. A new wrinkling testing method is developed and it is capable of applying in-plane biaxial compression and out-of-plane bending to represent wrinkling conditions in spinning. By evaluating strain increments of the un-supported flange and constructing strain diagrams representing the strain evolution during spinning, new insights into strain limits, wrinkling initiation and growth are attained. It is observed when the circumferential strain of the top surface of the un-supported flange cyclically increases to become and remain tensile, wrinkling initiates. The wrinkling initiation is a consequence of a rapid accumulation of the circumferential strain of the un-supported flange under cyclic loading induced by the roller, when the roller feed per mandrel revolution exceeds a limit. Subsequent roller feeding to the edge of the flange and wrinkling growth on the flange cause continued increases of the circumferential strain leading to the final wrinkling failure in spinning. The newly developed wrinkling test method has achieved wrinkling initiation and strain conditions similar to that observed in the early stage of the spinning process, which could be used as a guide to support the determination of the key process parameters for wrinkling-free spinning.

Highlights

- Investigating wrinkling mechanisms in spinning and effects of key process parameters.
- Evaluating strain accumulation and evolution that leading to wrinkling initiation.
- Developing wrinkling testing method by in-plane biaxial compression and out-of-pane bending.
- Wrinkling tests achieved strain conditions similar to early-stage wrinkling in spinning.

Keywords Shear spinning · Wrinkling · Finite element strain analysis · Wrinkling testing method

Terminology

- Mandrel rotation speed: rotational speed of the mandrel (rpm);
- Roller feed rate: roller linear velocity along the surface of the rotating blank (mm/min);
- Roller feed ratio: roller feed rate per revolution of the mandrel rotation (mm/rev);
- Feed ratio limit: maximum feed ratio beyond which wrinkling initiates (mm/rev);
- Winkling reference height: ideal height of the circumferential edge of the flange without wrinkling (mm);
- Wrinkling wave: one full wrinkling wave including one top and one bottom along the circumferential edge of the flange;
- Wrinkling wave amplitude: vertical distance between top and bottom of a wrinkling wave.

✉ Hui Long
h.long@sheffield.ac.uk

[1] School of Mechanical, Aerospace and Civil Engineering, the University of Sheffield, Sir Frederick Mappin Building, Sheffield S1 3JD, UK

Published online: 21 March 2026

1 Introduction

Sheet metal spinning is usually divided into conventional spinning and shear spinning, commonly used to produce axisymmetric products in various industrial applications. In conventional spinning, multi-passes are required for a roller tool to progressively deform a sheet blank to produce a desired geometry with unchanged blank thickness. In shear spinning, the blank thickness is reduced and multi-passes are not necessary. The process design of a shear spinning process includes decisions on the blank thickness reduction ratio and spinning process parameters such as roller feed rate and mandrel rotational speed. These depend on the geometry and material of a spun product required.

Wrinkling was considered as a common process failure in spinning process development [1]. A few studies stated that wrinkling could be considered as a plastic buckling failure, and the material deformation mode depended on the local curvatures and thickness of the sheet blank [2, 3]. An earlier study by Kobayashi [4] reported that the material deformation modes in the conventional spinning process were similar to those in the deep drawing process. It stated that wrinkling was caused by buckling due to compressive circumferential stresses occurring in the flange. A subsequent study by Hayama et al. [5] reported that the deformation modes during wrinkling were more complex and involved tension, compression, shearing and cyclic bending. Further investigations reported that wrinkling in shear spinning was different to deep drawing since the circumferential stress was uniform around the flange in deep drawing, but it was non-uniform in spinning because of the indentation created by the roller movement [6]. The wrinkling in spinning usually occurs at the edge of the un-spun flange of the sheet blank at a certain stage of the spinning process, and it becomes severer when the roller moves further away from the clamp and closer to the edge of the blank. Further studies reported that under some process conditions, minor wrinkles on the flange that occurred during previous roller passes of spinning could be flattened in the subsequent roller passes [7, 8]. However wrinkles normally could not be flattened in other sheet forming processes once they occurred; this is because the sheet blank in the spinning process is subjected to cyclic loading caused by the roller.

In an effort to understand the material deformation mechanics leading to wrinkling initiation in spinning processes, theoretical, analytical, finite element (FE) simulation and experimental methods have been developed. A theoretical wrinkling prediction model was proposed by determining the critical circumferential stress in conventional spinning based on a generalised variational principle of limit analysis [9]. It concluded that once the compressive circumferential stress during spinning exceeded its critical value, flange wrinkling occurred. An analytical model integrated with toolpath design for wrinkling prediction in conventional spinning was reported in [10]. The model was capable of creating processing maps showing the limits of key spinning parameters on the onset of the wrinkling, including toolpath profile, blank thickness, spin ratio and feed ratio. In a FE and experimental study of a multi-pass conventional spinning, it was observed that more complicated stress patterns of the un-spun flange of the blank showing both local and global bending due to cyclic roller contacts during spinning [8]. It was found that circumferential stresses were compressive on the flange near the local forming zone worked by the roller however these changed into tensile stresses when the blank rotated away from the roller [8]. To investigate effects of various process parameters on wrinkling in spinning, FE simulations of a conventional spinning process using the Box-Behnken design of experiments were developed [11]. It concluded that the wrinkling was caused by the build-up of residual bending moments, with the collapse of the flange being initiated by the formation of a plastic hinge between the roller and edge of the blank [11]. It was found that the roller feed per mandrel revolution produced the most significant effect on the onset of wrinkling [11]. By identifying the key spinning parameters, the effect of the feed ratio, defined as the roller feed rate per revolution of the mandrel rotation, on wrinkling was investigated in [12, 13]. In their experimental tests [13], an excessive feed ratio was the predominant factor to trigger wrinkling, and the wrinkling severity was also increased with a higher feed ratio. It was observed that wrinkling occurred when the applied feed ratio exceeded a feed ratio limit. The feed ratio limit was confirmed for the process setup of their study. However, this critical parameter varies with the processing conditions, including the geometry and the material of a spun part.

To date, no standardised testing method is in place to obtain the spin ability or forming limit of spinning processes to predict and prevent wrinkling. Only a handful of studies proposed testing methods to investigate wrinkling initiation in spinning. A buckling test was developed by Yoshida [14] to investigate the tendency of wrinkling formation of metal sheets; and wrinkling was created by applying uniaxial tension on the two ends of the specimen. Kim et al. [15] conducted a modified Yoshida buckling test by applying tension on the two ends of the specimen to investigate the effects of geometry and stress ratio on wrinkling initiation and growth. Strains and wrinkling height results were obtained from their tests using specimens with different widths and gripping distances. Cao et al. [16, 17] developed a wedge strip wrinkling test to investigate the onset of the buckling using a uniaxial tensile test machine to achieve various boundary conditions and stress ratios. It was concluded

that the strain needed to trigger the buckling was relatively small, and the buckling was very sensitive to compression of the sheet. From these studies, it is clear that the specimen design and boundary conditions are crucial for achieving the desired deformation states for initiating buckling. It was found by Kim et al. [15] that different specimen dimensions under identical loading conditions had resulted in different deformation states of the material. In the studies reported in [15] and [17], the wrinkling tests were conducted by using a uniaxial tensile test machine, which was carried out by applying uniaxial tension to each specimen. However, FE simulation studies reported in [8, 11] demonstrated that the wrinkled blank during spinning was subjected to multiaxial loading conditions including tension, bending, and shearing under cyclic loading. Therefore, the existing wrinkling test methods are not suitable for studying wrinkling mechanisms and predicting the onset of wrinkling in spinning processes.

In the study of material deformation under multiaxial loading conditions, a continuous bending under tension (CBT) test was developed by Emmens et al. [18, 19], in which a roller set continuously worked over the gauge area of a uniaxial tensile specimen, applying both tension and cyclic bending to the specimen. Further developing the CBT testing method, a tension under cyclic bending and compression (TCBC) was developed by Ai et al. [20]. The test rig design had one more roller installed on the roller set than that in the CBT test to provide a compression to the specimen therefore enabling both cyclic bending and compression loading during tension of the specimen. To enable in-plane two dimensional deformation, a biaxial tension under bending and compression (BTBC) test was further developed by Ai and Long [21], in which multiaxial deformation conditions were applied to a cruciform specimen enabling loading four arms rather than two of the specimen in the CBT and TCBC tests [18, 20]. However, these multiaxial tests aimed to investigate material behaviour under cyclic loading which eventually led to necking and fracture of the tested specimens; they are not capable of providing in-plane compression loading required for wrinkling testing in spinning.

Forming limit diagram (FLD) has been widely employed in sheet metal forming to establish the safe and potential failure zones during material deformation under different strain paths [22]. An international standard was first published in 2008 [23] and recently updated in 2021 [24]. The ISO 12004-2:2021 provides guidelines for conducting tests for the determination of forming-limit curves (FLCs) in the laboratory conditions for metallic sheet and strip materials. The FLCs can be obtained by designing standard specimen geometries which represent the material deformation under equi-biaxial tension, plane strain, uniaxial tension, and their intermediate strain states [24, 25]. Various studies employed the FLD to test the forming limit of specific materials for sheet forming applications, such as for stretch forming [26] and deep drawing [27, 28] processes. For example, in deep drawing process of a cylindrical cup, the bottom of the cup experiences equi-biaxial tension, the wall section was under plane strain, and the flange edge of the cup was under uniaxial compression which was more likely to cause wrinkling failure [27]. However, Emmens et al. [29] suggested that a FLD was only effective in predicting the material formability when the plane stress was the primary loading condition when a linear strain path was applied. In spinning processes, the material is under multiaxial and cyclic loading conditions imposed by the roller, the existing FLD methods in the ISO standard using Marciniak test or Nakajima test [24] are not suitable for spinning wrinkling tests. In the experimental study by Hayama et al. [5], it was found that the compression and tension deformation states of the flange were cyclically changing throughout the shear spinning process, depending on the location of the roller. Furthermore, the material deformation of the un-spun flange in shear spinning is not pure shear but a combination of shearing and bending as the roller moves to the edge of the blank to deform the material which induces cyclical bending and unbending of the flange near the roller contact zone.

It is clear there is a need to understand wrinkling initiation mechanisms in order to develop standardised methods to test strain limits in order to predict and prevent wrinkling failure for efficient spinning manufacturing. This study firstly develops finite element (FE) models of a shear spinning process to simulate wrinkling initiation under different process conditions, validated by spinning experimental tests. Strain variations of the un-supported flange during spinning are evaluated; strain evolution and strain diagram are obtained to identify strain conditions and their limits leading to wrinkling initiation. Secondly, a new wrinkling testing method is developed in this study aimed to produce wrinkling initiation similar to that in the spinning process. Experimental wrinkling tests are performed by developing two specimen designs and a wrinkling test rig capable of applying loadings for in-plane biaxial compression and out-of-plane bending. Corresponding FE models of these wrinkling tests are also developed to evaluate strain conditions for comparison with that from the FE spinning process simulations. The process limit and strain conditions that initiate wrinkling in spinning are identified and mechanisms of wrinkling initiation and growth are proposed. The developed wrinkling test method has achieved a close correlation of the wrinkling condition comparable to that occurred in the early-stage of the spinning process. The strain conditions and limits obtained from the wrinkling test method could be used to guide the determination of the key process parameters, and the feed ratio, in spinning processes.

2 Analysis of strain evolution and wrinkling initiation in spinning

To understand the material deformation during wrinkling, FE simulation models of a shear spinning process under different process conditions are developed to evaluate wrinkling initiation and investigate strain evolution. Shear spinning experiment is also developed to validate the FE simulation of the onset of wrinkling. Strain limit diagrams leading to wrinkling initiation are obtained and evaluated.

2.1 Finite element methods of wrinkling simulation in spinning

The simulation of a metal spinning process, as illustrated in Fig. 1a, is a highly dynamic problem that involves a rotating mandrel with a rotational speed commonly over 1000 rpm. The spinning process time is relatively short, usually having a spinning duration of 10 s. The contact condition between the roller and the blank is complex and the material of the blank experiences the nonlinear plastic deformation. The roller movement is defined by boundary conditions to simulate the loading induced by the roller while the mandrel and the blank rotate together, which results in the material plastic deformation of the blank to obtain a desired geometry of the spun part. FE software Abaqus/Explicit is selected to simulate the shear spinning process and the main loading and boundary conditions are shown in Fig. 1a. Aluminium alloy AA5251-H22 is used as the blank material in the FE simulation of the shear spinning to form a conic part of 45°, details of the assembly and component design are provided in Appendix A. The material flow stress curve used in the FE spinning simulation is obtained experimentally and it is included in Appendix B.

The continuum shell element type in Abaqus, SC8R, is selected for the blank with one layer of elements in the thickness direction to optimise the required mesh density and computational efficiency. To prevent the hourglass problem from occurring at the flange of the blank due to bending, a number of meshing strategies are explored to select the final mesh as shown in Fig. 1b. The mass scaling method has to be applied in the FE spinning simulation due to extremely small time increments as a result of excessively small element sizes and a short spinning duration. Different values of the mass scaling factor of 9, 16, 36, 49 and 64 are tested and the value of 36 is selected to ensure that the dynamic effect due to the artificially increased material density has not affected the simulation accuracy but still achieves sufficient computational efficiency. The total number of elements of the blank is 56,000 and the CPU time to complete one simulation model of the spinning process is over 256 h.

The contact condition used in this study by Abaqus/Explicit is the surface-to-surface contact, defined by the penalty contact algorithm and Coulomb's friction law. Three contact interactions are defined, these are: the roller with the top surface of the blank, the backplate with the top surface of the blank, and the mandrel with the bottom surface of the blank, as illustrated in Fig. 1a. The value of coefficient of

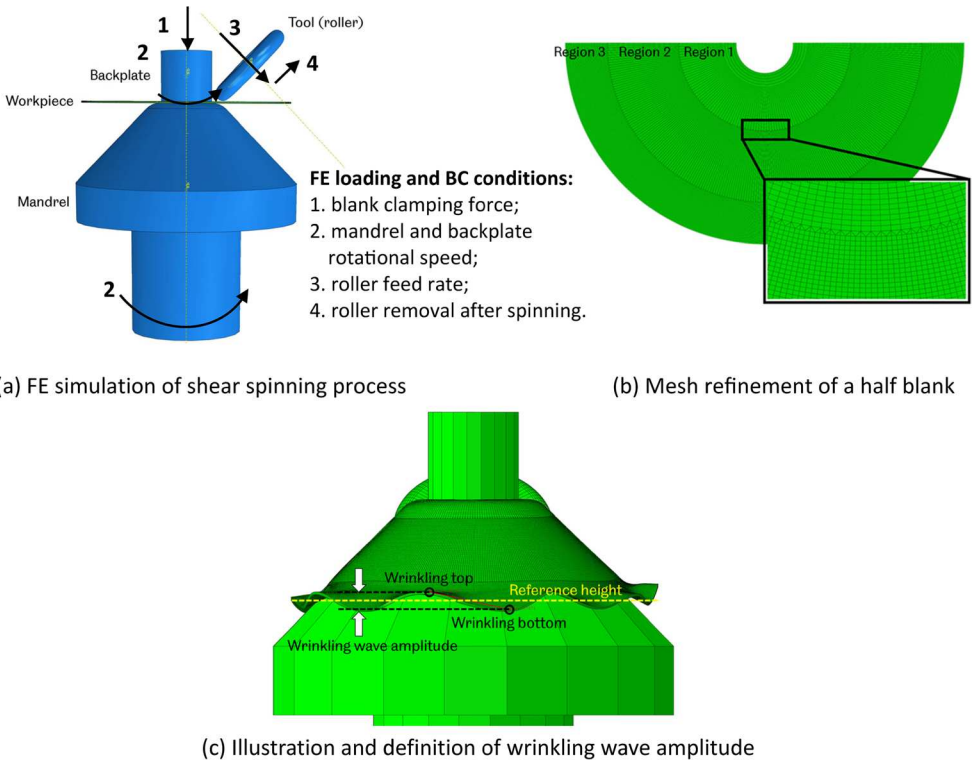

(a) FE simulation of shear spinning process

(b) Mesh refinement of a half blank

(c) Illustration and definition of wrinkling wave amplitude

Fig. 1 Finite element simulation of wrinkling in shear spinning process

Table 1 FE simulation models in shear spinning of AA5251-H22 sheet (thickness 1 mm)

FE Model No.	Mandrel rotational speed (rpm)	Roller feed ratio (mm/rev)	Simulated WWA (mm)	Final No. of wrinkling waves	Wrinkling initiation time (s)	Spinning time (s)	Modelled spinning time before mesh distortion (s)
1	200	1.5	6.85	8	3.32	10.8	7.17
2	1000	0.3	-	-	WF	10.8	10.8
3	1000	0.4	-	-	WF	8.1	8.1
4	1000	0.5	-	-	WF	6.48	6.48
5	1000	0.75	3.05	7	2.38	4.32	4.32
6	1000	1.0	3.48	8	1.68	3.24	3.24
7	1000	1.25	6.24	9	1.01	2.592	1.793
8	1000	1.3	6.32	8	0.922	2.492	1.705
9	1000	1.4	6.51	8	0.796	2.016	1.563
10	1000	1.5	6.75	10	0.736	2.16	1.373

WF Wrinkling free, *WWA* Wrinkling wave amplitude

friction for each of these contacts is 0.02, 0.5, 0.5, respectively [8].

In the spinning process, when the roller feed ratio exceeds a limit for a specific sheet material and thickness of a desired geometry, wrinkling occurs. The roller feed ratio, in a unit of mm/rev, is defined as the roller feed rate divided by the mandrel rotational speed. To investigate the effect of key process parameters on the wrinkling initiation and progression during the shear spinning process, a total of 10 FE models is constructed, as shown in Table 1, with varied values of the mandrel rotational speed and roller feed ratio. To evaluate the effect of the feed ratio on wrinkling, the roller feed rate is varied and two different values of the mandrel rotational speed are adopted in these simulations.

In this study, wrinkling wave amplitude (WWA) is proposed to quantify wrinkling severity in spinning. The WWA is defined as the vertical distance between top and bottom surface points of a wrinkle wave along the circumference edge of the flange, as shown in Fig. 1c. When without wrinkling, the WWA is zero thus the circumference edge of the flange is at the same position as the reference height. If wrinkling occurs, the details of wrinkling wave amplitude and number of wrinkling waves are recorded, as shown in Table 1. If no wrinkling occurs, it is recorded as wrinkling-free (WF). Because wrinkling can result in excessive FE mesh distortions, some FE simulations cannot be completed to their actual spinning time; these are also recorded in Table 1.

2.2 Experimental validation of FE simulation of wrinkling in spinning

To validate FE simulation results of the shear spinning process, spinning experimental tests are developed and conducted. The tests are conducted by using a modified AJAX Premier 200 CNC turning centre, with a capacity of axial and radial feed rates up to 3000 mm/min and a mandrel rotational speed up to 2300 rpm, covering the required range of the process parameters used in the FE simulation models of the shear spinning process. Roller vibrations during the spinning process are measured by employing the similar measurement method developed in [10] to detect wrinkling initiation time. Wrinkling is considered to be initiated when waveform amplitudes of the roller vibration are increased beyond the stable range of the roller vibration amplitudes without wrinkling during spinning. The spinning experiment conditions are shown in Table 2 which have the same process parameters as that of FE model No. 1, 6 and 7 respectively.

As shown in Fig. 2, wrinkling always occurs around the circumferential edge of the un-supported flange of the blank in a form of wrinkling waves with tops and bottoms. To measure wrinkling quantitatively, both wrinkling wave amplitude and number of wrinkling waves from the FE simulation and the spinning experiment are compared. Table 2 shows the comparison of wrinkles generated under different values of the roller feed ratio and mandrel rotational speed.

Table 2 Comparison of experimental measured and FE simulated wrinkling wave amplitude (WWA)

Test No.	FE Model No.	Mandrel rotational speed (rpm)	Feed ratio (mm/rev)	Measured WWA (mm)	Simulated WWA (mm)	Measured/FE modelled No. of wrinkles	Normalised/actual wrinkling initiation time (s)
1	1	200	1.50	7.69	6.85	8/8	0.75/8.25
2	6	1000	1.00	3.44	3.48	8/8	0.65/2.11
3	7	1000	1.25	6.75	6.24	8/9	0.63/1.63

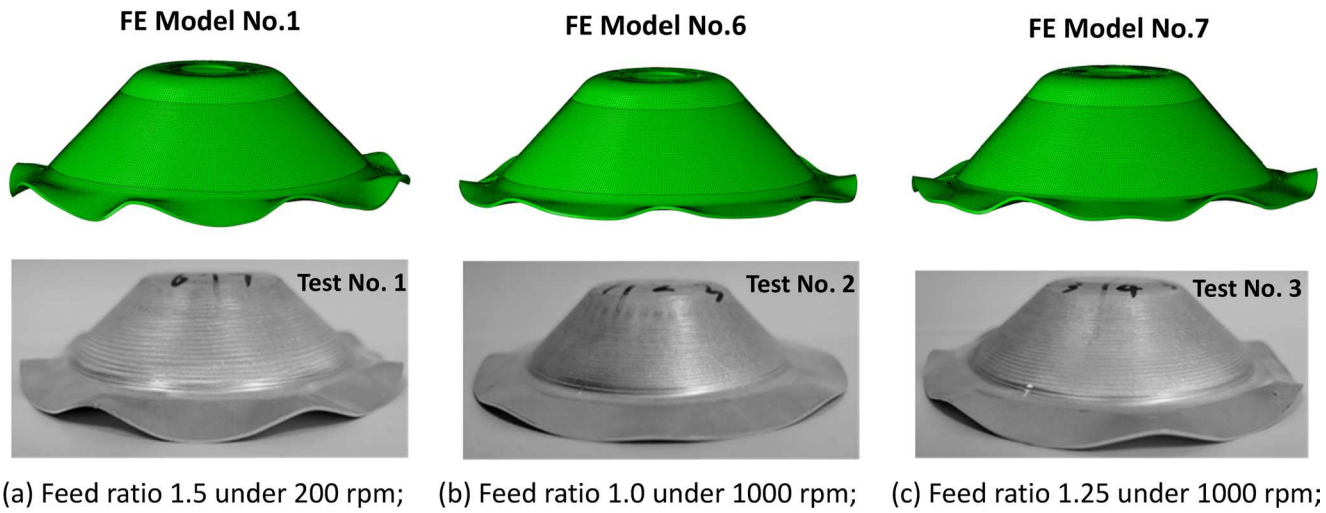

Fig. 2 Comparison of wrinkled spun parts between FE simulation and experiment

The roller feed ratio determines if wrinkling occurs in spinning as well as the severity of wrinkling and resulting WWAs, as summarised in Tables 1 and 2. It is clear that a higher roller feed ratio results in a great WWA. Comparing WWAs and number of wrinkling waves of FE Model No.1 and Test No.1; FE Model No.6 and Test No.2; FE Model No.7 and Test No.3; respectively, the FE simulation and experimental results under the same process parameters show very good agreements. Different mandrel rotational speeds with the same feed ratio result in different spinning times. For a direct comparison, the normalised wrinkling initiation time of each spinning process, along with the actual wrinkling initiation time, are summarised in Table 2.

Previous studies did not investigate the connection between the dynamic effect in spinning and the wrinkling initiation. In this study, this effect is investigated by developing FE Models No.1 and No. 10 under the same feed ratio of 1.5 mm/rev but a different mandrel rotational speed of 200 rpm and 1000 rpm, respectively. It has been observed that these two spinning processes, with an identical feed ratio but different mandrel rotational speeds, show an identical wrinkling initiation time, 3.32 s for FE Model No.1 and 0.736 s for FE Model No.10, five times difference, the same as the difference of the mandrel rotational speed of these two models. The WWAs, 6.85 mm for FE Model No.1 and 6.75 mm for FE Model No.10, are also similar when the feed ratio is the same but with a different mandrel rotational speed. If a spinning process with a feed ratio is wrinkling-free, the outcome of any other spinning processes with the same feed ratio but with proportional changes in the mandrel rotational speed and roller feed rate will also be wrinkling-free. The same conclusion is true for minor or severe wrinkling cases, respectively. The feed ratio determines the onset of wrinkling as well as the wrinkling severity in the subsequent spinning process when the roller continues deforms the blank, similar to the observations of the previous studies reported in [11, 13].

2.3 Wrinkling initiation and effect of roller feed ratio

In this section, the circumferential strain is firstly selected to evaluate the effect of the roller feed ratio on wrinkling initiation in the spinning process. Variations of the circumferential strain on the top surface at the edge of the un-supported flange of the blank are analysed. Generally, over the same period of time, under a higher feed ratio, a greater increase of the circumferential strain is observed at the top surface of the flange edge, as shown in Fig. 3. Three outcomes related to wrinkling of the flange are identified from the FE simulations of the spinning process under different values of the feed ratio, these are: severe wrinkling (FE Models No.7 to No.10); minor wrinkling (FE Models No.5 and No.6); and wrinkling-free (FE Models No. 2 to No.4).

FE results of Models No.7 to No.10 show excessive FE mesh distortions due to severe wrinkling of the flange therefore the results of the circumferential strain after excessive mesh distortions are not included in Fig. 3. FE results of Models No.5 and No.6 show that minor wrinkling waves are initially formed on the flange but they are flattened by the roller during the subsequent stage of the spinning process when the roller works on these minor wrinkling waves directly. This phenomenon has also been observed in the spinning experiment, reported in [7, 8]. FE results of Models No.2 to No.4 show no wrinkling waves formed on the flange therefore the spinning process is wrinkling-free. As can be seen in Fig. 3, for a wrinkling-free spinning process (FE Models No.2 to No.4), it is clear that the circumferential strains on the top surface at the edge of the flange remain compressive throughout the spinning process. Small tensile

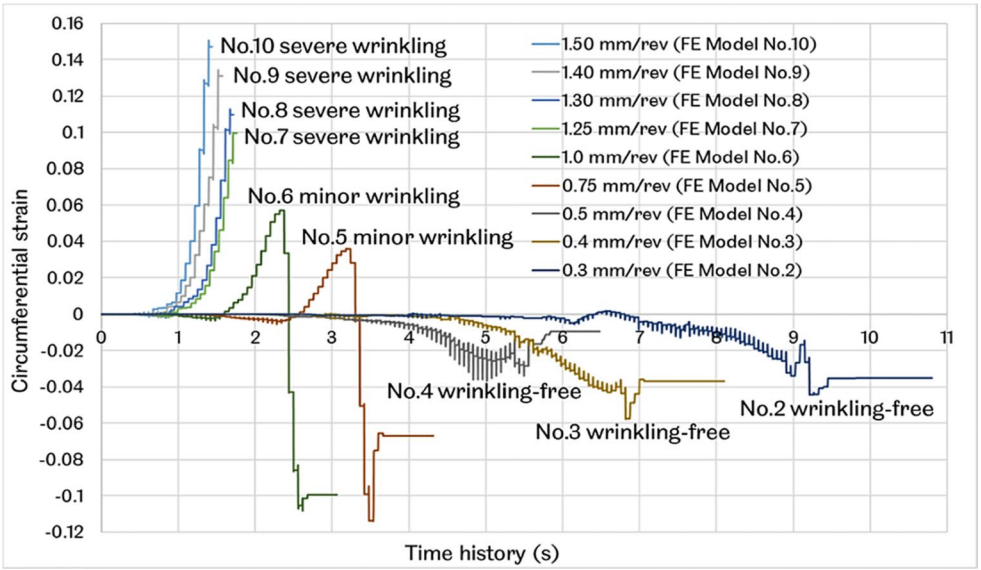

Fig. 3 Variations of maximum circumferential strain of top surface at the edge of the flange under different values of spinning feed ratio

circumferential strains may occur but they change back to compressive strains after the blank rotating away from the area locally deformed by the roller.

In this study, the feed ratio limit is defined as the maximum feed ratio applied in spinning leading to a wrinkling-free process. For the process parameters and spinning process considered in this study, the feed ratio limit is observed to be 0.5 mm/rev from the FE simulation results shown in Fig. 3. This observation is validated by the spinning experimental tests. Beyond this feed ratio limit, wrinkling occurs. The obvious pattern is that the greater the feed ratio is, the higher the tensile circumferential strain occurs on the top surface of the un-supported flange. For a spinning process severely wrinkled, for example, FE Model No.10, Fig. 4 shows gradual increases of the tensile circumferential strain on the top surface at the edge of the un-supported flange, from very small maximum strain values, around 0.0345, which continuously increases after each roller feed per mandrel rotation, finally reaches the maximum tensile strain of around 0.1. At spinning time 1.355 s, the maximum tensile strains can be seen on the top surface of each wrinkling wave across the entire circumference of the up-supported flange, leading to severe wrinkling. In contrast, for a spinning process with a feed ratio lower than the feed ratio limit (0.5 mm/rev in this study), as shown in FE Models No.2 to No.4, the circumferential strain increases slower than that of the FE models with a high feed ratio. For these models, the circumferential strain on the top surface of the flange remains to be compressive during the whole spinning process, as shown in Fig. 3.

To investigate strain variations at the critical stage in spinning under different feed ratio conditions which leading to different wrinkling outcomes, i.e. wrinkling-free, minor wrinkling and severe wrinkling, FE Models No.4, 5, 6 and 7 are selected for a detailed comparison of the maximum circumferential strain on the top surface at the edge of the un-supported flange. As shown in Fig. 5, it can be seen that the noticeable strain variation starts after 0.7 s and cyclically changes when the roller deforms the blank cyclically in the nearby area of the flange section considered. For the wrinkling-free case (FE Model No.4), the circumferential strain on the top surface of the flange remains compressive throughout the spinning process. For the severe wrinkling case (FE Model No.7), the circumferential strain is initially compressive but increases gradually to become completely tensile just after 0.9 s; this trend continues until the occurrence of excessive mesh distortions at 1.7 s in spinning. For the minor wrinkling cases (FE Models No. 5 and 6), the circumferential strain is also initially compressive and increases gradually to become tensile just after 1.5 s (For Model No.6) and after 2.5 s (For Model No.5). However, the trend of tensile strain increases only lasts less than 1 s then the circumferential strain changes back to be compressive and it remains compressive throughout until the end of the spinning process.

From the above analysis, it can be concluded that when the roller feed ratio applied is greater than the feed ratio limit, 0.5 mm/rev in this study, the maximum circumferential strain of the top surface at the edge of the un-supported flange rapidly increases to become tensile and remains tensile during the spinning process, wrinkling initiates. A higher feed ratio results in greater rapid increases of the circumferential strain, resulting in greater severity of wrinkling. For a wrinkling-free case, the maximum circumferential strain of the top surface at the edge of the un-supported flange remains compressive throughout the spinning process.

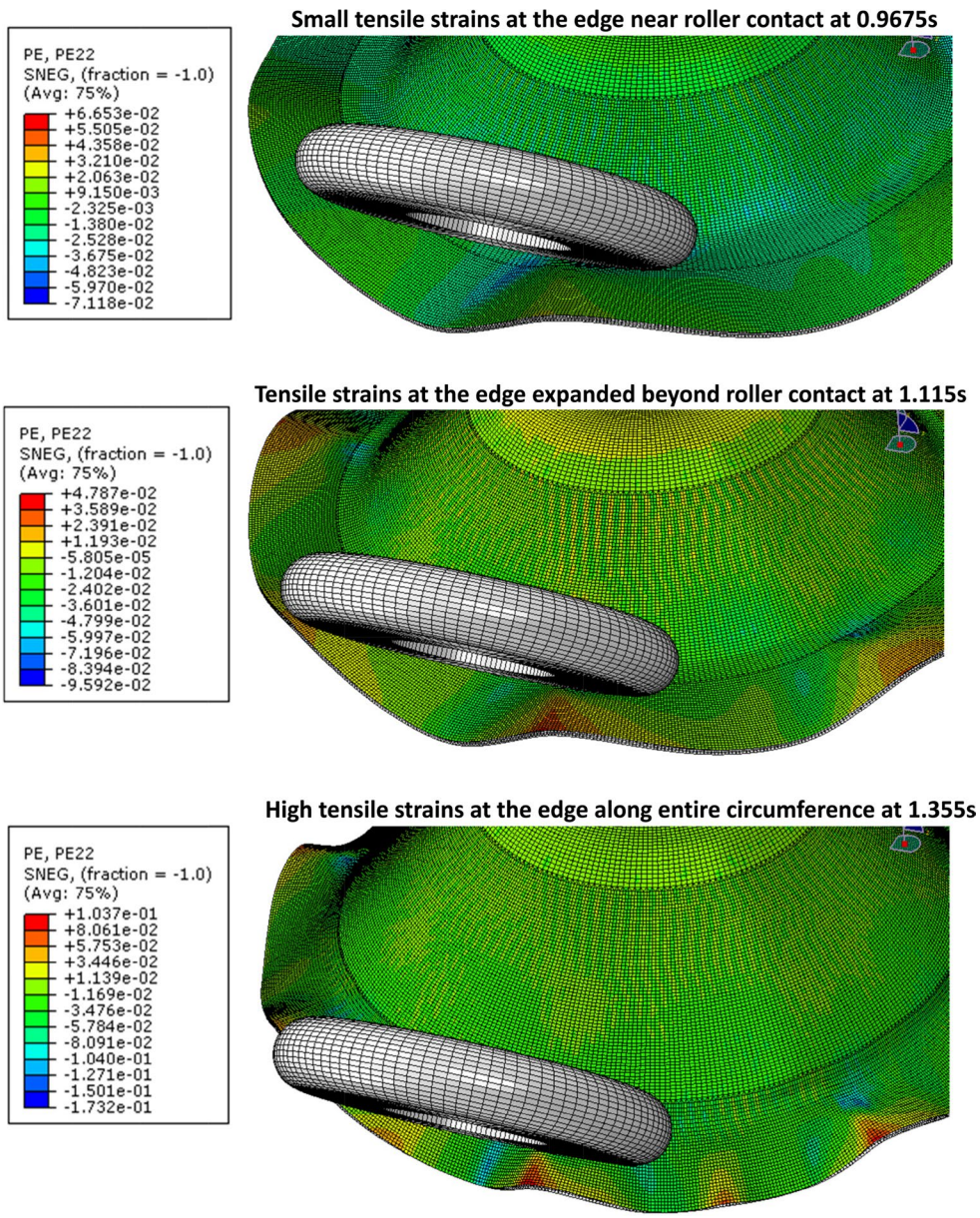

Fig. 4 Tensile circumferential strains of top surface with severe wrinkling, FE Model No.10

2.4 Evaluation of strain evolution in spinning

As observed in the previous studies [27], wrinkling also occurred in other sheet forming processes. For example, in deep drawing, excessive compressive circumferential stresses buckle the flange of the blank resulting in wrinkling. To evaluate strain evolutions from the start of the spinning process to the formation of wrinkles, FE Model No. 10 is selected for detailed analysis, for which severe wrinkling has occurred. The maximum circumferential and radial strains on the top and bottom surfaces at the edge of a wrinkling top of the un-supported flange are analysed, as shown in Fig. 6. In Fig. 6a, it depicts the variation of the strains with spinning time. In Fig. 6b, it shows the evolution of the ratio of the radial strain to the circumferential strain, from the wrinkling initiation stage to spinning time 1.373 s, before excessive mesh distortions have occurred. Although nine integration points are assigned in the thickness direction of the blank in a single layer of continuum shell elements in Abaqus, only the results from the nodes on the top and bottom surfaces can be outputted. It is clear that the un-supported flange is under localised bending due to the action of the roller deforming the nearby flange of the blank. Due to the localised roller bending effect, the wrinkling top surface of the un-supported flange is elongated resulting in tensile circumferential strains. The wrinkling bottom surface of the un-supported flange is compressed resulting in compressive circumferential strains.

There is an obvious pattern that the strains of the edge of the un-supported flange increase continuously as the

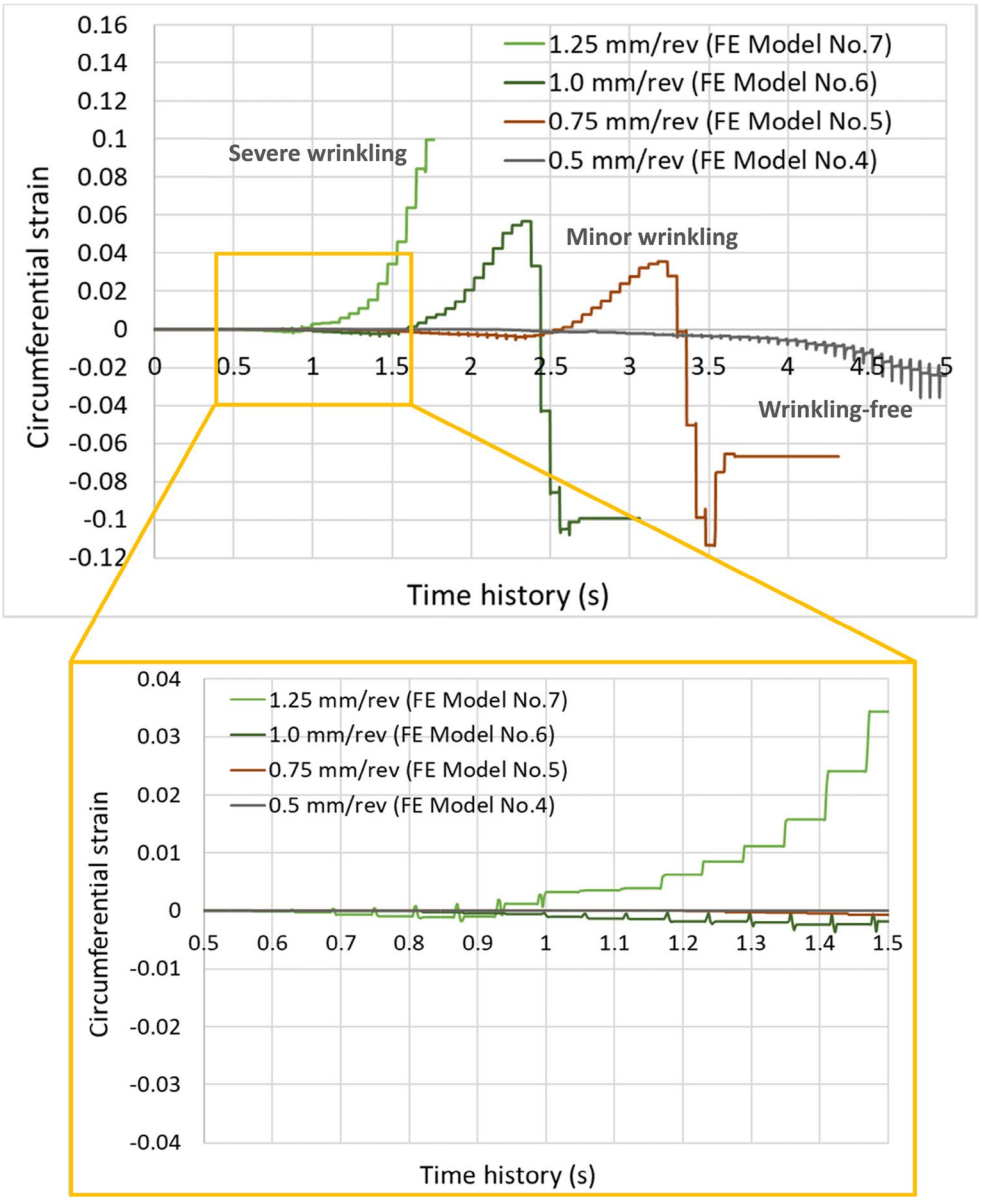

Fig. 5 Comparison of variations of the maximum circumferential strain for spinning processes with wrinkling-free (Model No.4), minor wrinkling (Models 5 & 6), and severe wrinkling (Molde No.7)

spinning process proceeds when the roller deforms the blank material gradually, as shown in Fig. 6a. There is a small strain increment after each deformation cycle by roller feed per mandrel revolution. Moreover, the deformation of the blank material caused by the roller is highly localised. After moving away from the current roller contact area, the strains of the edge of the un-supported flange remain unchanged until the next mandrel revolution when the roller deforms the nearby area of the blank again. From Fig. 6b, it can be seen that the ratio of the radial strain (RS) to the circumferential strain (CS) of the bottom surface of the un-supported flange edge is positioned near the uniaxial compression zone of the strain diagram, while the RS/CS ratio of the top surface of the un-supported flange edge is positioned near the uniaxial tension zone of the strain diagram. The RS/CS ratios of both surfaces have correctly reflected the strain paths of wrinkling top and wrinkling bottom of the wrinkled flange.

2.5 Strain diagram and wrinkling mechanisms

From the results shown in Figs. 3, 4 and 6 and evaluations in Sect. 2.3 and 2.4, the wrinkling initiation is a consequence of a rapid accumulation of the circumferential strain at the edge of the un-supported flange during the deformation of the nearby area of the blank by the roller, due to a large roller feed per mandrel revolution greater than its limit. To further evaluate the evolution of the circumferential strain and radial strain that leading to wrinkling initiation, a node set on the top surface of the wrinkled flange in FE Model No.10

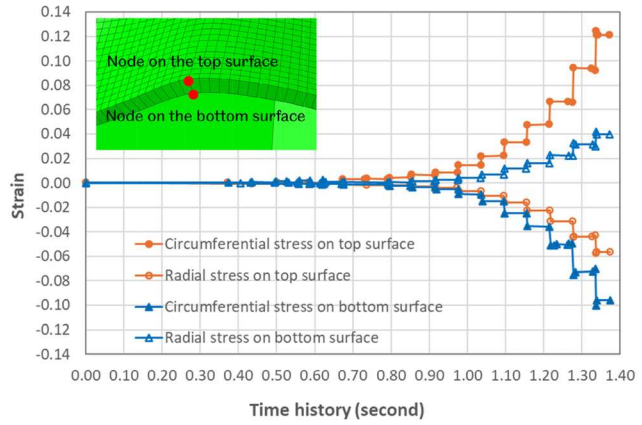

(a) Time history of circumferential and radial strains

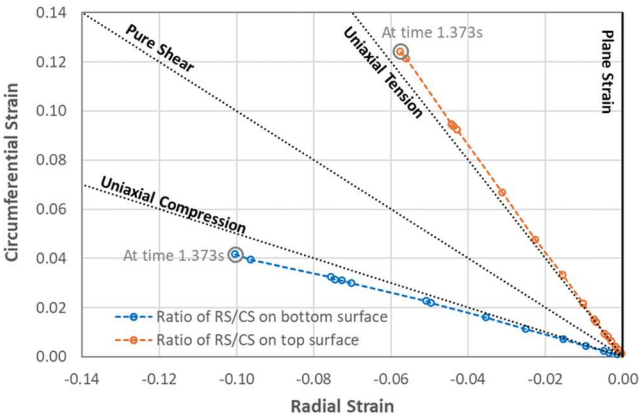

(b) Ratio of radial strain (RS) to circumferential strain (CS)

Fig. 6 Strain variation of top and bottom surfaces at the edge of wrinkled flange, FE Model No. 10

is selected, numbered from 1 to 14, where the maximum circumferential and radial strains have occurred. The strain diagram is drawn by using the radial strain as minor strain and the circumferential strain as major strain, as shown in Fig. 7. At the early stage of the spinning process, the circumferential strain and radial strain at the top surface of the wrinkled flange are compressive, however they propagate to a wider space on the strain diagram starting after the 13th mandrel revolution (0.7725 s) and leading to severe wrinkling in the later spinning stage of the 23rd mandrel revolution. There is an obvious pattern that the strain space is gradually expanded after each mandrel revolution because the blank material has been continuously deformed by the roller. The circumferential and radial strains on the wrinkling top (nodes No. 1 ~ 14) are mostly positioned between strain paths from − 1/2 to 1 (from uniaxial tension to equal-biaxial tension). For these selected nodes, the closer to the edge of the un-supported flange, the greater the circumferential strain, occurred at node No.14, as shown in Fig. 7.

The most important observation from the strain diagram analysis is that the wrinkling is caused by the strain accumulation during each contact between the roller and deformed flange section, creating a local bending effect of the un-supported flange section along the circumferential direction of the blank. The feed ratio determines the roller feed distance per mandrel rotation and the degree of the material deformation thus it governs the amount of strain accumulated on the un-supported flange following each roller contact. The wrinkling initiation is a result of the un-supported flange being deformed beyond a strain limit by the roller due to an excessive feed ratio applied to the blank. An excessive feed ratio leads to a rapid increase of the maximum circumferential strain of the top surface that becomes tensile and remains tensile during the subsequent roller feeding, resulting in wrinkling initiation. Continued roller feeding to the edge of the flange and wrinkling growth on the flange cause further increases of the circumferential strain leading to the final wrinkling failure in spinning. The identification of the wrinkling initiation and growth mechanisms is essential for developing a new wrinkling test method to obtain strain limits to prevent wrinkling in spinning.

3 Development of new wrinkling testing method

The international standards have been established to determine forming-limit curves for predicting material deformation failures in sheet metal forming processes, such as Nakajima and Marciniak testing methods in the ISO EN12004-2:2021 [24]. However, there is no wrinkling testing method available to predict strain limits for the onset of wrinkling in spinning processes. In this section, the development of a wrinkling testing method is presented aiming to produce wrinkling initiation similar to that in the spinning process so that to predict wrinkling strain limits.

3.1 Wrinkling testing method and specimen design

As observed and discussed in Sect. 2, wrinkling is localised in the un-supported flange. The dynamic effect in spinning, due to higher feed rate and higher mandrel rotational speed, shows no effect on wrinkling initiation, as long as they change proportionally to maintain the feed ratio unchanged, as discussed in Sect. 2.2. Therefore, the flange deformation leading to wrinkling can be treated independently when developing the wrinkling test method.

Two specimen designs for wrinkling testing are developed, as illustrated in Fig. 8. The gauge area of each specimen is designed to have an identical geometry to the actual arc section of a wrinkled flange in spinning, illustrated by the overlapped arc section in Fig. 8. Specimen design details

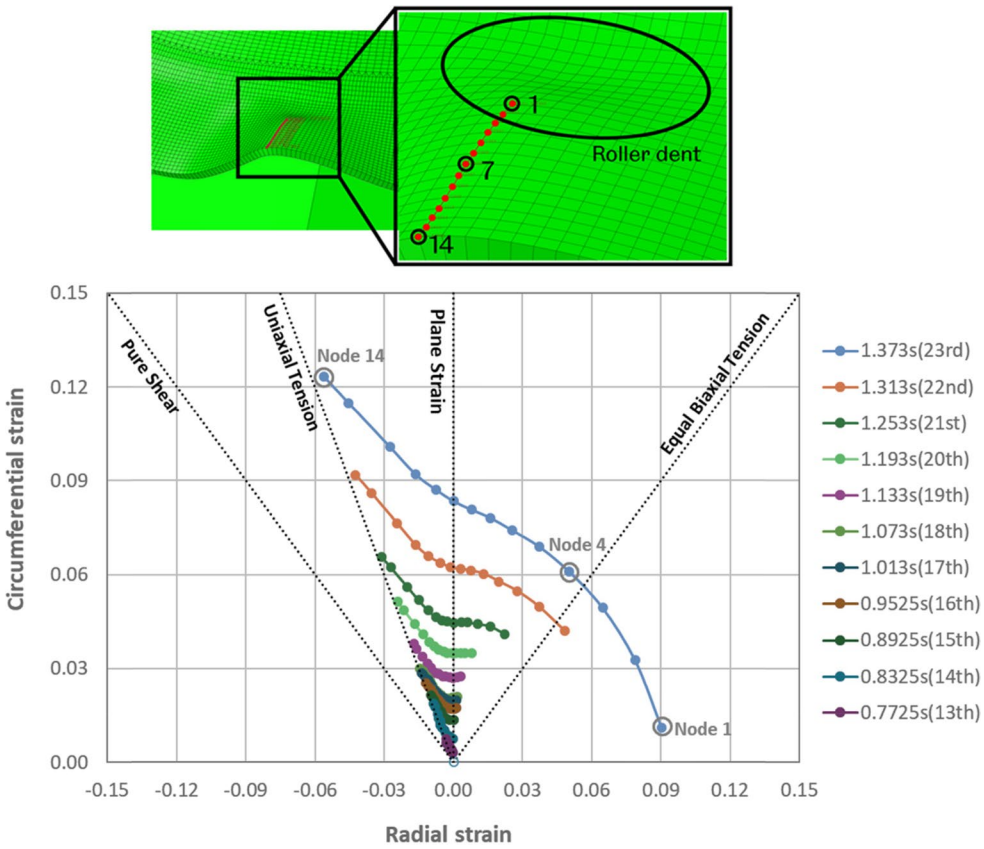

Fig. 7 Strain diagram of top surface of wrinkled flange, FE Model No. 10

are provided in Appendix C. For Specimen Design 1, the corresponding loadings are applied through the two arms of the specimen, as illustrated in Fig. 8a. However, in spinning, three sides of the arc section of the flange are constrained by the adjacent material, marked as red-lined boundaries, while the outside edge of the flange is free from any constraint. This consideration leads to the development of Specimen Design 2, as shown in Fig. 8b. In both designs, the thickness of the gauge area is reduced to make the gauge area less resistant to compressive loading therefore to ensure the specimen always wrinkles in the gauge area. The material of the specimen is AA5251-H22, the same as that used for the spinning experiment and FE simulation as presented in Sect. 2.

3.2 Experiment of wrinkling tests

The proposed wrinkling test method requires in-plane biaxial tension/compression deformation when the specimen is also subjected to bending and compression loading in the out-of-plane direction. The rig developed by Ai and Long in [21] is modified to adopt the new design of wrinkling test method developed in this study. The modified rig can apply loading conditions and boundary constraints to the specimens designed for the wrinkling test experiment, to ensure similar loading conditions as that by the roller deforming the un-supported flange in the spinning process. Figure 9 shows the winkling test rig and its main components.

Four groups of wrinkling tests are conducted as outlined in Table 3. For specimen design 1 in tests No.1 and No.2, the in-plane compression loading is applied by a 0.12 mm/s compression speed on both arms of the specimen along axis 1 for 10 s. A total of 2.4 mm compression displacement is applied to the specimen to cause the specimen to wrinkle within the gauge area. For specimen design 2 in tests No.3 and No.4, an additional constraint is applied to the third arm of the specimen fixed by the clamp on axis 2 throughout the testing process. After the in-plane compressive loading, the out-of-plane bending loading is applied using the bending tool with a 5 mm radius hemispherical head via the handwheel by applying a downward movement. This loading bends the wrinkled specimen back to its initial horizontal plane. To determine strains after testing, the laser grid etching method is applied, as suggested in the ISO EN12004-2:2021 [23, 24]. Laser etched circle lines, in a diameter of 1 mm, are created on the gauge area of each specimen, as shown in Fig. 10.

3.3 Finite element simulation of wrinkling testing

Corresponding to the wrinkling experiment as outlined in Table 3, four FE simulation models of the wrinkling tests of

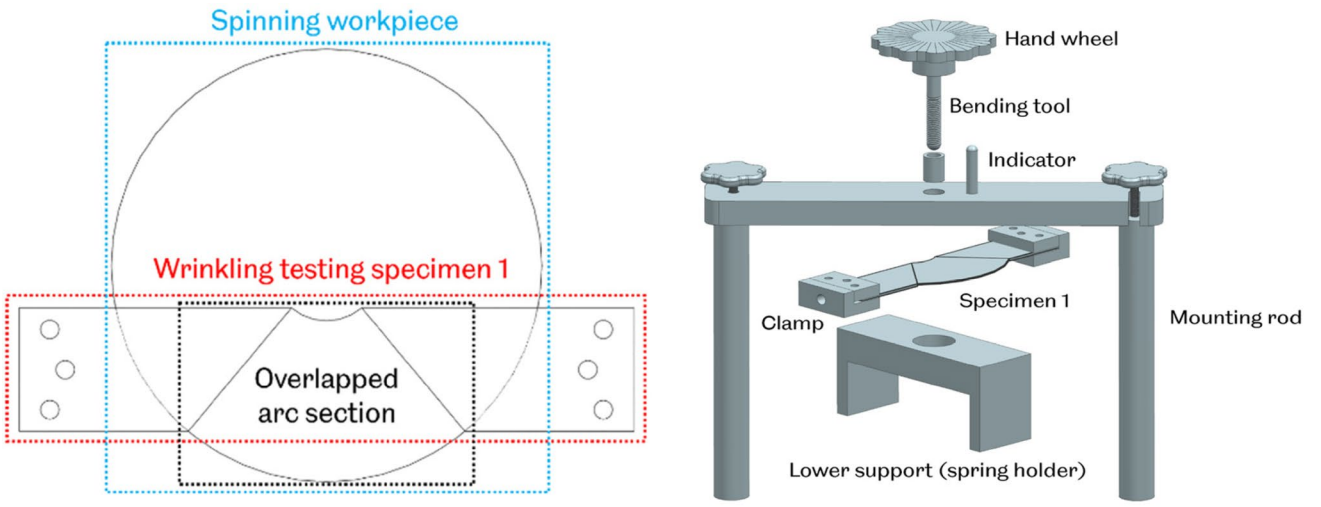

(a) Specimen Design 1 for wrinkling test and illustration of loading and constraints

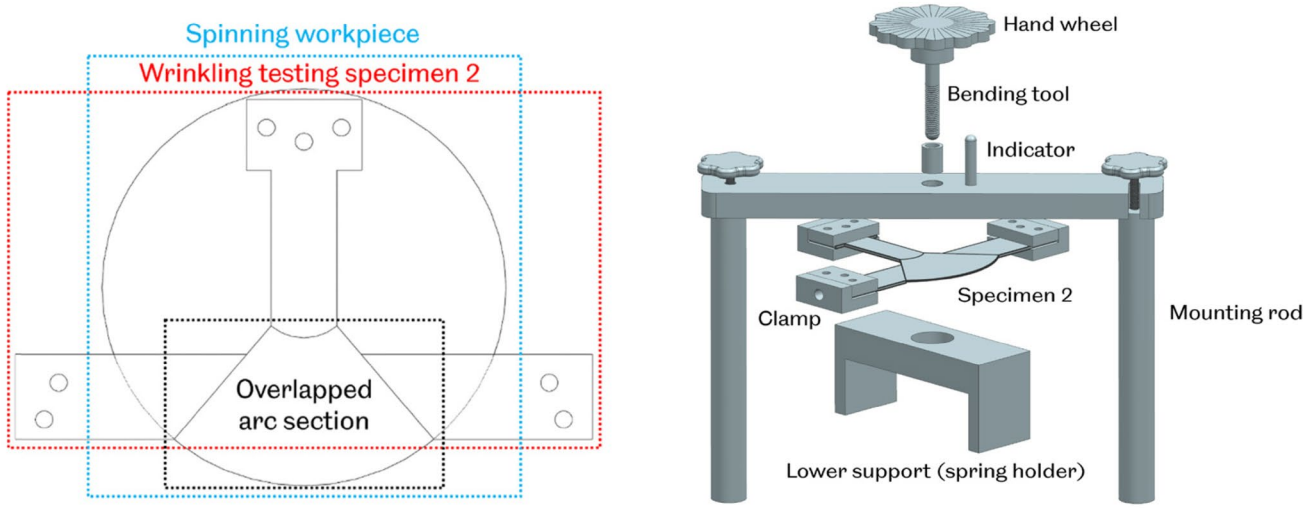

(b) Specimen Design 2 for wrinkling test and illustration of loading and constraints

Fig. 8 Development of wrinkling testing method and specimen design

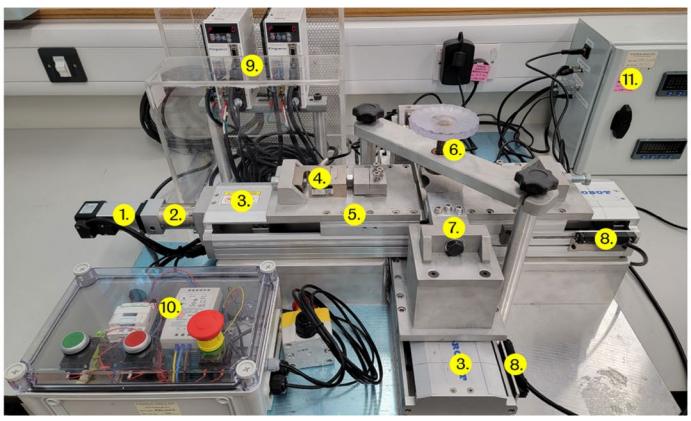

1. motor;
2. gearbox;
3. slider;
4. load cell;
5. carriage;
6. bending system;
7. clamp;
8. displacement sensor;
9. motor speed control units;
10. power control box;
11. signal interpreting unit.

Fig. 9 Wrinkling test rig capable of in-plane biaxial tension & compression with out-of-plane bending

Table 3 Experimental wrinkling tests and specimen loading conditions

Test No.	Specimen Design	Loading on axis 1	Displacement on axis 2	Loading from bending tool
1	1	Compression	-	-
2	1	Compression	-	Bending (after compression)
3	2	Compression	Fixed	-
4	2	Compression	Fixed	Bending (after compression)

the two specimen designs are developed to simulate wrinkling formation under the same loading and boundary conditions as that in the wrinkling experiment. For specimen design 1, in FE test model 1, displacements on the arms of specimen 1 are eliminated thus the deformation only concentrates on the thickness-reduced gauge area. In FE test model 2, a bending tool is introduced to induce bending deformation of the specimen after wrinkles occur in the gauge area of the specimen, acting as the action of the roller compressing the wrinkled flange in the spinning process. The FE mesh, loading and boundary conditions of FE test models 1 and 2 are detailed in Table 3; Fig. 11. For specimen design 2, it has a T-shape geometry with a thickness-reduced arc-shaped gauge area connected to three arms of the specimen. In FE test model 3, only in-plane compressions are applied to the specimen; while for FE test model 4, both in-plane compressions and out-of-the plane bending are applied to the specimen. The details of loading and boundary conditions are given in Table 3; Fig. 12.

4 Wrinkling test results and discussion

Wrinkling test results and FE strain diagram for specimen design 1 and 2 under different loading and boundary conditions are presented in Figs. 13 and 14, respectively. Strain values from the corresponding FE wrinkling simulation of the spinning process (FE model No. 10), at two stages of

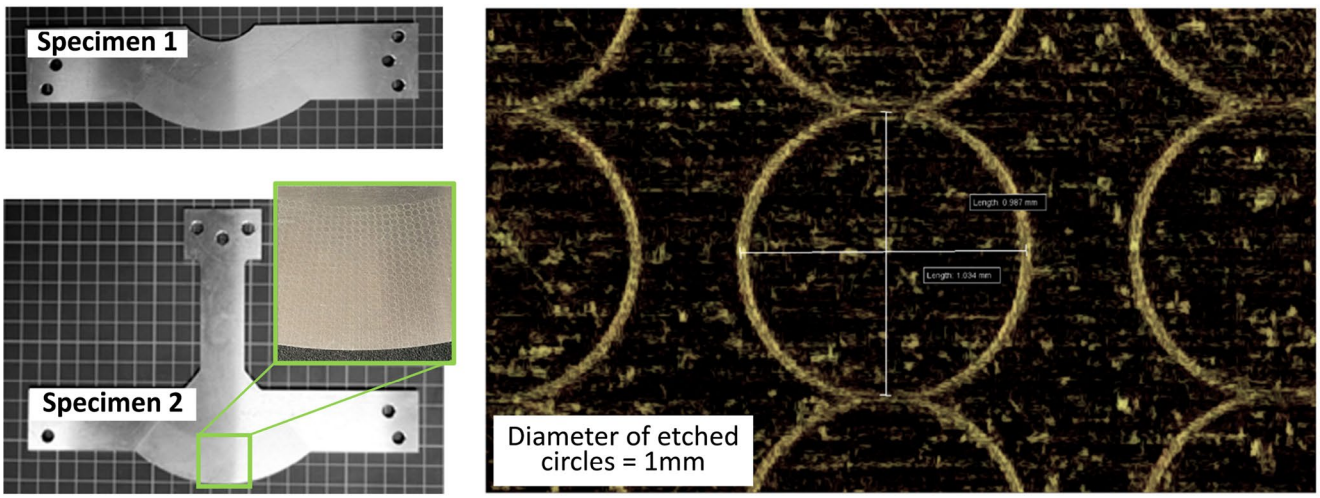

Fig. 10 Winkling test specimens 1 and 2 and laser etching for strain measurements

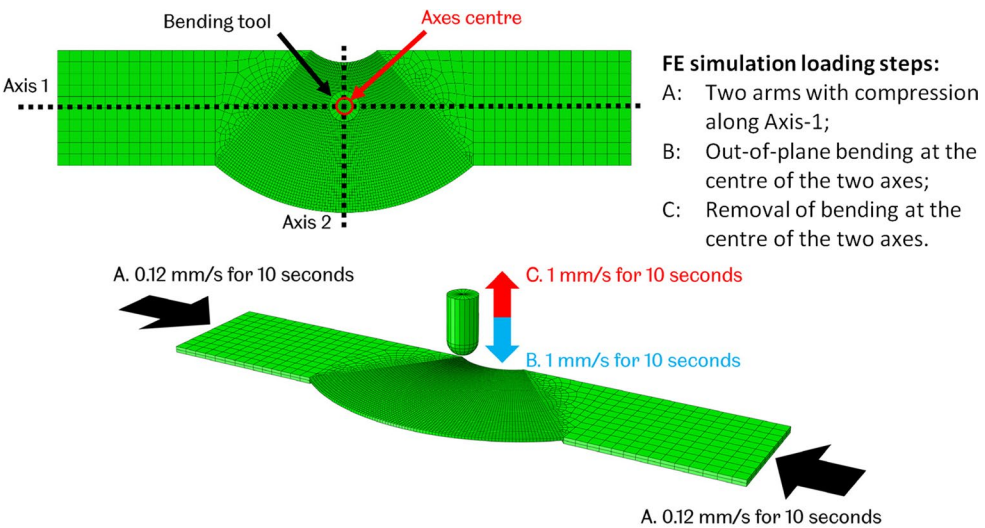

Fig. 11 Loading conditions of wrinkling test of specimen design 1, FE test No.1 and No.2

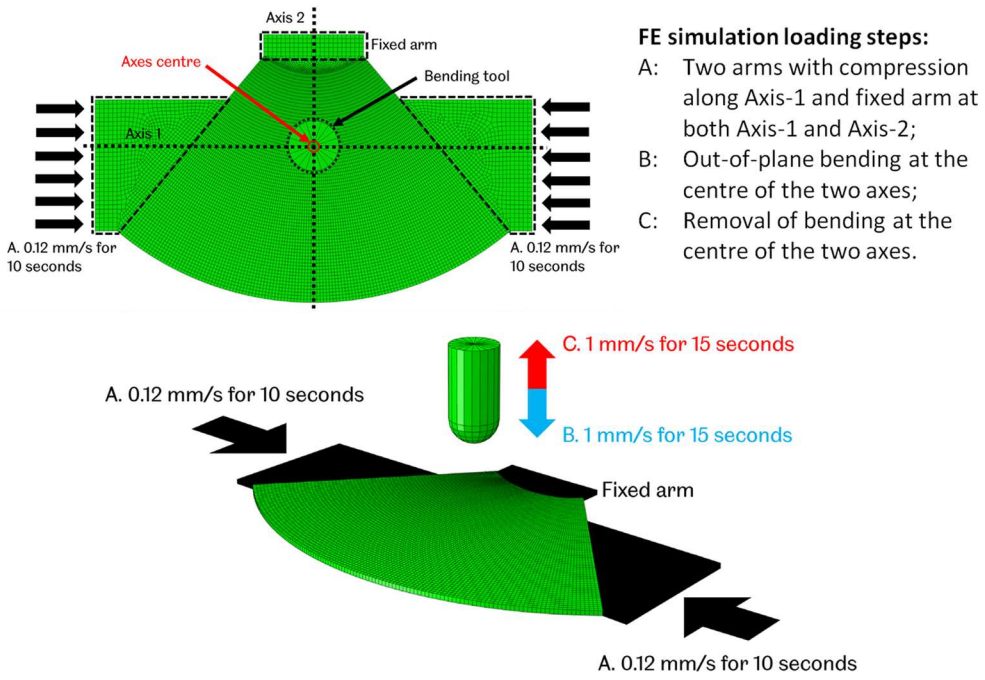

Fig. 12 Loading conditions of wrinkling test of specimen design 2, FE test No. 3 and No. 4

the 19th and 23rd mandrel revolution, are also presented together with the wrinkling test results for comparison. As shown in Fig. 13a, by comparing the circumferential strain of the FE wrinkling test No.1 of specimen design 1 with that of the FE spinning process model No.10, it is clear that the wrinkling test simulates an earlier stage of the wrinkling development, close to the 19th mandrel revolution in the spinning process.

In the FE simulation of wrinkling test No.2 of specimen design 1 shown in Fig. 13b, by employing the bending tool, it creates a dent on the specimen surface, similar to that in the spinning process. When compared with the FE wrinkling test No. 1, the circumferential strains of the FE wrinkling test No.2 are slightly closer to that of the 19th mandrel revolution in the FE spinning model No. 10. However, the edge of the specimen design 1 has not reached higher strain conditions, not high enough to be comparable to that in the final stage of the spinning process in the 23rd mandrel revolution. This may be because the compression applied by the bending tool to the arc gauge area is evenly distributed, not localised enough to produce sufficient compression to induce a greater circumferential strain to the edge of the specimen in the wrinkling test. The strains measured from the wrinkling tests are scattered in the strain diagram due to difficulties to obtain accurate measurements of the deformed circles etched on the specimen. However, the measured strains from the wrinkling Test No.2 show a better correlation with that of the FE wrinkling test simulation at 19th mandrel revolution, mostly located between the strain path between −1/2 and 0, as shown in Fig. 13b.

For wrinkling tests No.3 and No.4 of specimen design 2, the FE circumferential strains and their comparison with that of the FE simulation of the spinning process are presented in Fig. 14. The difference between wrinkling tests No.3 and No.4 with tests No.1 and No.2 is the additional constraint of the third arm of specimen design 2. The width of the first two arms of the arc gauge area in specimen 1 is reduced in specimen 2 to only cover the partial size of the wrinkled flange in the spinning process. The compression of the bending tool in wrinkling test No.4 of specimen design 2 is only applied to the partial arc gauge area thus the bending is not as severely as that in specimen design 1 in test No.2. From the FE strain results of wrinkling test No.3 shown in Fig. 14a, it can be seen that the circumferential strain distribution at the top surface has a maximum value of 0.033 at the edge of the wrinkle top surface.

For the wrinkling test FE model No.4 in Fig. 14b, the bending tool applied to specimen design 2 with the third arm as an additional boundary constraint has created one fully completed wrinkling wave with one wrinkling top and one wrinkling bottom, similar to that in the spinning process. A maximum circumferential strain of 0.016 from the wrinkling test No.4 occurs at the edge of the specimen. The strain diagram of the wrinkling test No.4 is similar to that in the earlier stage of the spinning process, at the 14th or 15th mandrel revolution as simulated by FE spinning model No.10, shown in Fig. 14b. The strains measured from the wrinkling tested specimens are also scattered around strain paths between −1 and 0. A better correlation with that of the FE wrinkling test simulation is observed for specimen

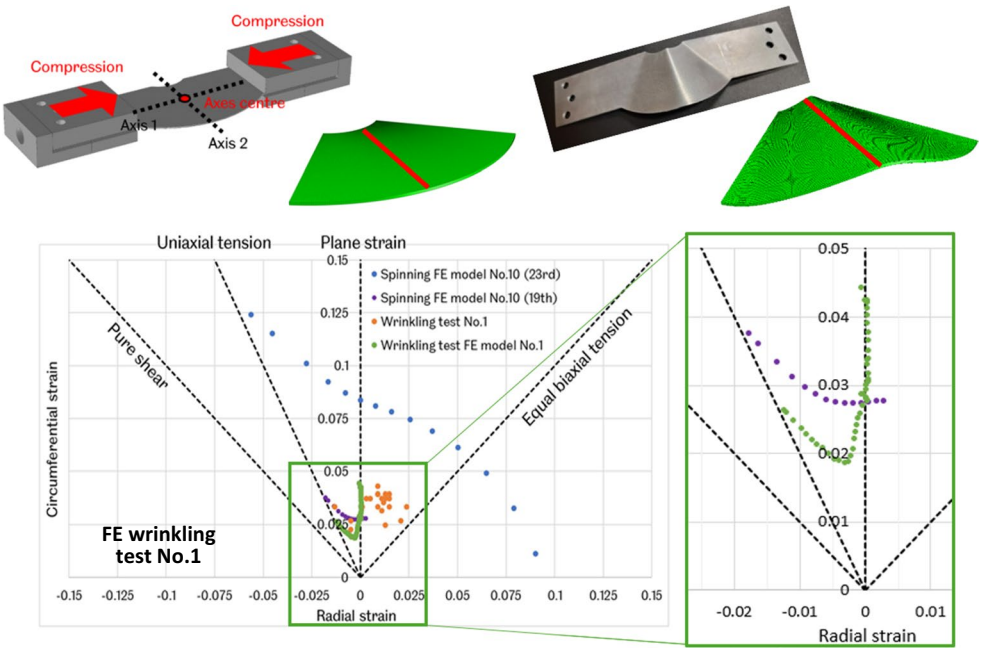

(a) Experiment and FE strain diagram of specimen 1 Test No.1 without bending tool

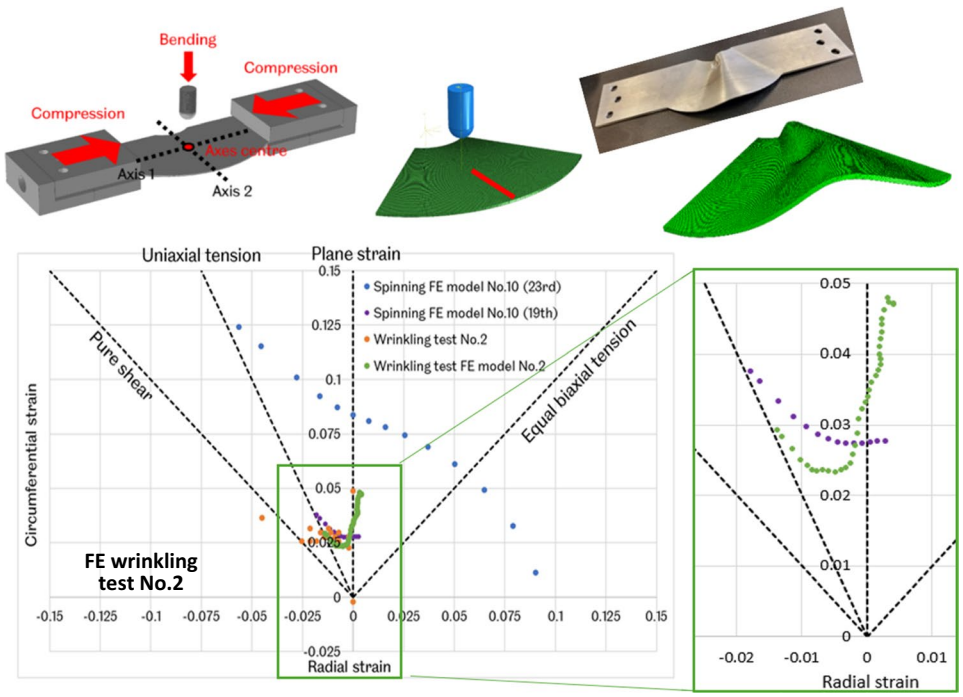

(b) Experiment and FE strain diagram of specimen 1 Test No.2 with bending tool

Fig. 13 Wrinkling test and FE simulation results of specimen 1, compared with FE spinning model No. 10

design 2 (Fig. 14) in comparison with specimen design 1 (Fig. 13).

Figure 15 shows the comparison of circumferential stress distributions obtained from wrinkling test No.4 with that from the spinning process of FE spinning model No.10. Different to other three wrinkling tests No.1, 2, and 3, the FE simulation of the wrinkling test No.4 shows that the bending tool creates tensile circumferential stresses adjacent to the bending tool contact but the circumferential stress is compressive at the roller contact zone. The loading of the bending tool has started to create a full wrinkling wave with top and bottom in the un-supported flange around the

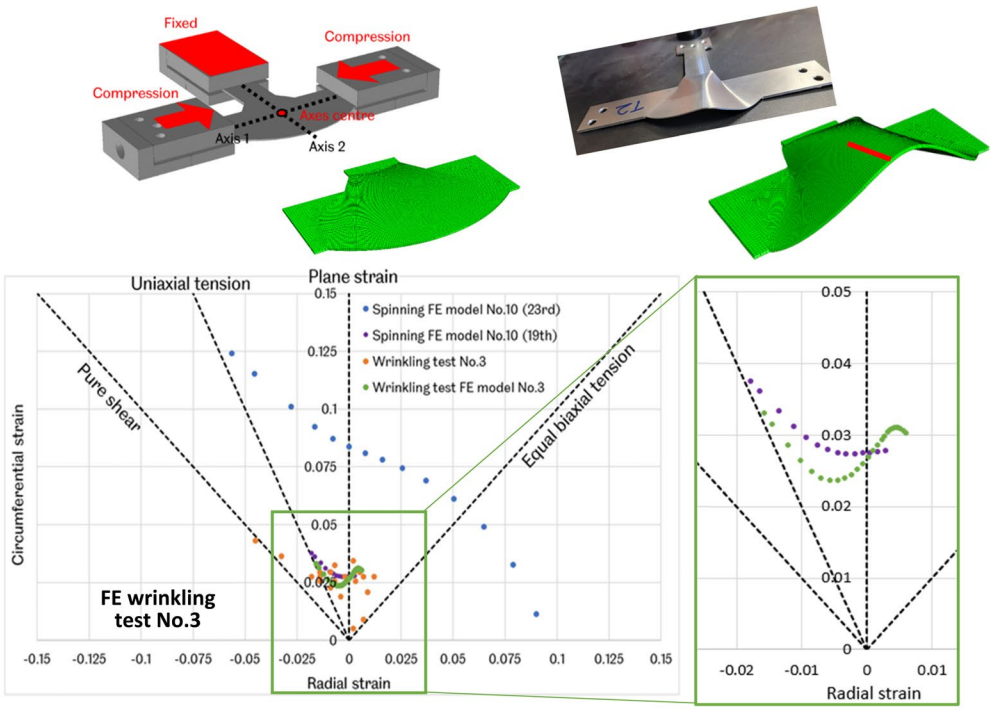

(a) Experiment and FE strain diagram of specimen 2 Test No.3 without bending tool

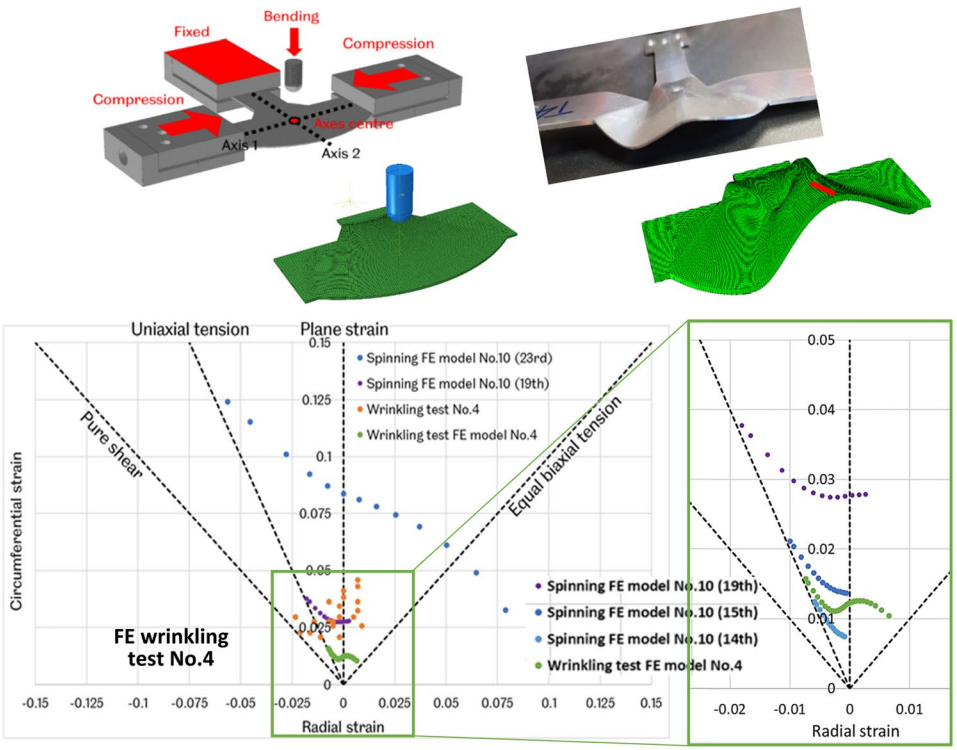

(b) Experiment and FE strain diagram of specimen 2 Test No.4 with bending tool

Fig. 14 Wrinkling test and FE simulation results of specimen 2, compared with FE spinning model No. 10

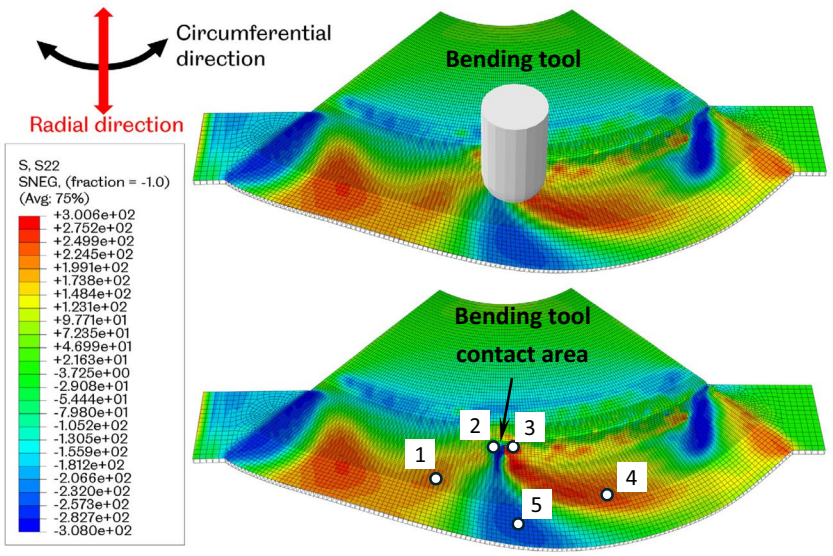

(a) FE wrinkling test model No.4 at bending tool contact, time at 5 seconds

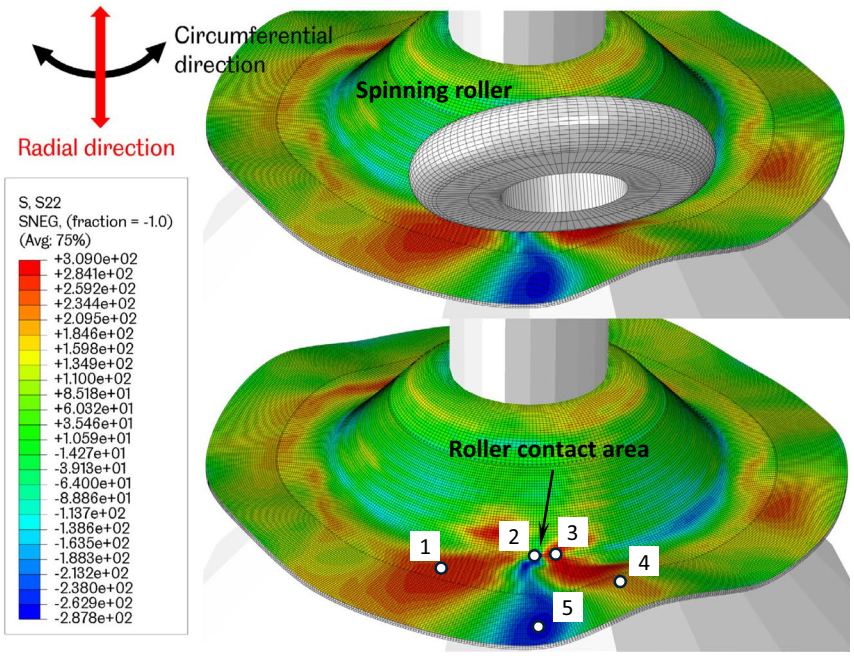

(b) FE spinning simulation model No.10 at roller contact, time at 0.75 seconds

Fig. 15 Comparison of circumferential stress distributions of wrinkling test and spinning process

bending tool, as shown in Fig. 15a. This is very similar to the flange deformation and circumferential stress distribution in the FE spinning simulation (FE Model No.10) shown in Fig. 15b. These are at the equivalent time of deformation in both processes, 0.75 s for spinning process and 5 s for wrinkling test. Table 4 shows a comparison of the maximum circumferential stress and strain in values at five selected areas, with the maximum stress deviation of 13.8%. As can be seen, both FE wrinkling test model No.4 and FE spinning model No.10 indicate a similar pattern of compressive circumferential stresses in Area-5 and tensile circumferential stresses at Area-1 and Area-4, creating a wrinkling wave.

As shown in Figs. 13 and 14, the circumferential strains of all the wrinkling tests based on specimen designs 1 and 2 are much smaller than the final strains at the 23rd mandrel revolution in the FE spinning model No.10. This

Table 4 Comparison of circumferential stress and strain of FE wrinkling test and FE spinning

Area No.	Stress: FE wrinkling test No.4 (MPa)	Stress: FE spinning model No.10 (MPa)	Deviation
1	223.5	254.4	13.8%
2	−293.5	−306.8	4.53%
3	294.2	312.4	6.19%
4	261.5	272.2	4.09%
5	−259.9	−262.5	1.00%
Area No.	Strain: FE wrinkling test No.4	Strain: FE spinning model No.10	Deviation
1	0.0028	0.0023	21.7%
2	−0.2446	−0.0547	>100%
3	0.0088	0.0072	22.2%
4	0.0161	0.0159	1.26%
5	−0.0073	−0.0066	10.6%

is considered to be the result of only one loading cycle being applied in each wrinkling test. However in the spinning process, the same area of the flange is worked by the roller over several loading cycles before the deformed area of the sheet blank moves towards the edge of the flange. If the developed wrinkling test rig could apply multiple loading cycles of in-plane compression to the two-sided arms and the out-of-plane bending to specimen 2 in test No.4, the circumferential strain at the edge of the arc gauge area of the specimen could be accumulated gradually to reach a higher strain values, as that observed in the FE spinning process, shown in Figs. 6 and 7. The maximum circumferential strain values which result in wrinkling, such as that obtained in wrinkling test No.4 using specimen design 2, could be used as a guide to determine the strain limit and key process parameters to prevent wrinkling in spinning.

5 Conclusions

In this study, the wrinkling initiation mechanisms and strain limits in shear spinning are investigated. A new wrinkling test method is developed; both experiment and FE simulation of the wrinkling tests are conducted to evaluate the strain evolution during wrinkling initiation. The strain diagrams from the FE spinning simulations and FE wrinkling tests are investigated. The main conclusions are:

1) Wrinkling initiation is a result of the un-supported flange being deformed beyond a strain limit by the roller due to an excessive roller feed per mandrel revolution applied to the blank in spinning. An excessive roller feed leads to a rapid increase of the maximum circumferential strain of the edge of the un-supported flange during each roller contact with the nearby deformed flange section;
2) When the maximum circumferential strain of the top surface of the un-supported flange becomes tensile and remains tensile during the subsequent roller feeding, wrinkling initiates. Continued roller feeding to the edge of the un-supported flange and wrinkling growth on the un-supported flange cause further increases of the circumferential strain leading to the final wrinkling failure in spinning;
3) The feed ratio is the most critical process parameter determining if wrinkling is to occur in a spinning process. When the feed ratio is greater than a certain limit, which is specific to the spinning material and process design, wrinkling is to occur. In this study, the feed ratio limit is found to be 0.5 mm/rev for the spinning process considered;
4) The dynamic effect in spinning is investigated by FE simulation and experiment of two testing conditions of the spinning process with the same feed ratio but different mandrel rotational speeds and roller feed rates. The higher roller feed rate and higher mandrel rotational speed applied do not affect the wrinkling initiation and severity, as long as the roller feed rate varies proportionally with the mandrel rotational speed to keep the feed ratio below the feed ratio limit;
5) To bridge the current research gap of lacking of standardised testing methods for predicting wrinkling initiation in spinning, a new wrinkling test method is proposed by developing two specimen designs which are evaluated by conducting both wrinkling test experiment and FE simulation;
6) Among the four types of the wrinkling tests performed, wrinkling test No.4 using specimen design 2, loaded by in-plane biaxial compression and out-of-pane bending using a bending tool, has achieved a closest correlation of the wrinkling initiation and strain conditions similar to that observed at the early stage of the spinning process;
7) The wrinkling tests have achieved the wrinkling initiation and early-stage wrinkling growth of that in the spinning process because of the application of only one pass/feed in the wrinkling tests. To achieve the same level of high circumference strains as that in the final wrinkling stage of the spinning process, multiple passes/feeds by using the bending tool is required;
8) This study identifies that the cause of wrinkling initiation in spinning is because of a rapid accumulation of the circumferential strain which resulted in permanent tensile strains of the top surface of the un-supported flange edge under cyclic loading induced by the roller, when the roller feed ratio exceeds a limit. The new wrinkling test method provides a new concept to further develop standardised wrinkling tests for preventing wrinkling in spinning processes.

Appendix A: Assembly of the shear spinning process and dimensions of main components

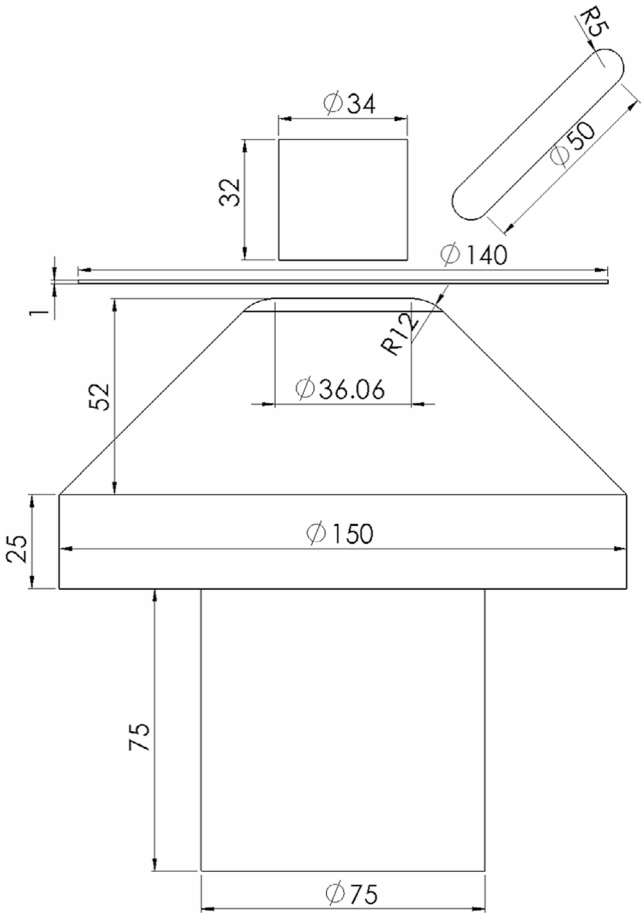

Appendix B: Flow stress of AA5251-H22 used in the FE spinning and FE wrinkling test models

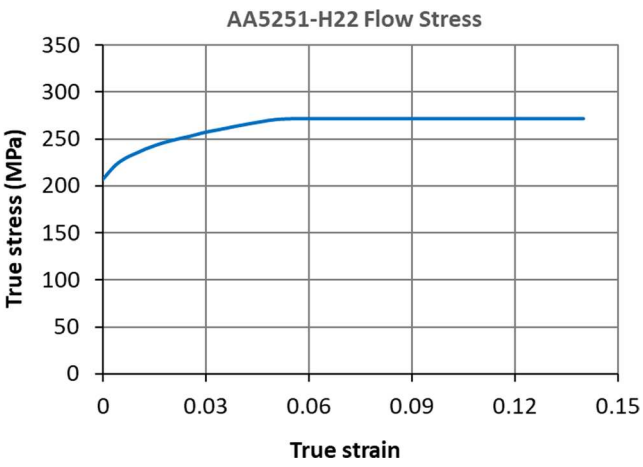

Appendix C: Specimen designs of wrinkling tests

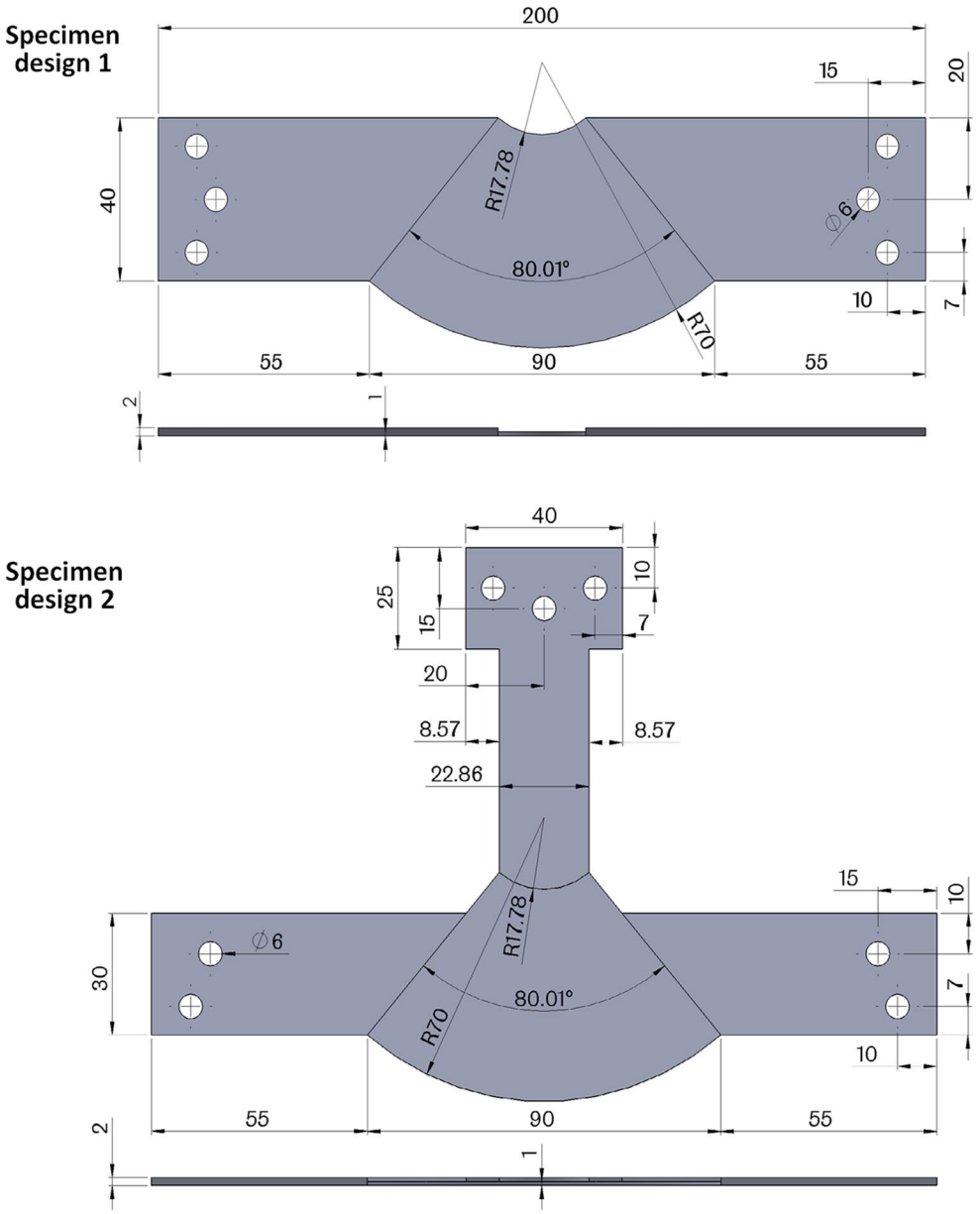

Acknowledgements The authors would like to thank technical support from Jamie Booth, David Webster and Chris Todd in the Department of Mechanical Engineering for developing the spinning experiment, and manufacturing and building the wrinkling testing rig.

Author contributions Z. Li: Conceptualisation, Methodology, Investigation, Formal Analysis, Validation, Visualization, Writing – original draft. H. Long: Conceptualisation, Methodology, Supervision, Writing – original draft, Writing – review and editing.

Declarations

Competing interests No funding was received for conducting this study. The authors have no competing interests to declare that are relevant to the content of this article.

References

1. Runge M (1994) Spinning and Flow Forming. Leifeld GmbH
2. Hutchinson JW (1974) Plastic Buckling. Advances in Applied Mechanics, 67–144. https://doi.org/10.1016/S0065-2156(08)70031-0
3. Wong CC, Dean TA, Lin J (2003) A review of spinning, shear forming and flow forming processes. Int J Mach Tools Manuf 43(14):1419–1435. https://doi.org/10.1016/S0890-6955(03)00172-X
4. Kobayashi S (1963) Instability in conventional spinning of cones,". J Manuf Sci Eng Trans ASME 85(1):44–48. https://doi.org/10.1115/1.3667585
5. Hayama M, Murota T, Kudo H (1966) Deformation modes and wrinkling of flange on shear spinning. Bull JSME 9(34):423–433. https://doi.org/10.1299/jsme1958.9.423
6. Hayama M, Kudo H, Shinokura T (1970) Study of the pass schedule in conventional simple spinning. Bull JSME 13(65):1358–1365. https://doi.org/10.1299/jsme1958.13.1358
7. Kawai K, Hayama M (1987) Roller pass programming in conventional spinning by NC spinning machine. In: Lange, K. (ed.), Advanced Technology of Plasticity, 2. Springer-Verlag 1987:711–718
8. Wang L, Long H (2011) Investigation of material deformation in multi-pass conventional metal spinning. Mater Des 32(5):2891–2899. https://doi.org/10.1016/j.matdes.2010.12.021
9. Chen SW, Zhan M, Gao PF, Mad F, Zhang HR (2021) A new robust theoretical prediction model for flange wrinkling in conventional spinning. J Mater Process Technol 288:116849. https://doi.org/10.1016/j.jmatprotec.2020.116849
10. Li ZH, Long H (2022) An analytical model integrated with toolpath design for wrinkling prediction in conventional spinning. J Mater Process Technol 300:117399. https://doi.org/10.1016/j.jmatprotec.2021.117399
11. Watson M, Long H, Lu B (2015) Investigation of wrinkling failure mechanics in metal spinning by Box-Behnken design of experiments using finite element method. Int J Adv Manuf Technol 78(5):981–995. https://doi.org/10.1007/s00170-014-6694-6
12. Hayama M, Yokohama National University (1981) Study on spin ability of aluminium and its alloys. Bull Fac Eng 30:63–72
13. Childerhouse T, Long H (2019) Processing maps for wrinkle free and quality enhanced parts by shear spinning. Procedia Manuf 29:137–144. https://doi.org/10.1016/j.promfg.2019.02.118
14. Yoshida K (1983) Purpose and feature of Yoshida buckling test (YBT). J Japan Soc Technol Plast 24:901–905
15. Kim JB, Yoon JW, Yang DY (2000) Wrinkling initiation and growth in modified Yoshida buckling test: finite element analysis and experimental comparison. Int J Mech Sci 42:1683–1714. https://doi.org/10.1016/S0020-7403(99)00046-6
16. Wang X, Cao J (2000) An analytical model for flange wrinkling in Sheet Metal Forming. J Manuf Process 2(2):100–107. https://doi.org/10.1016/S1526-6125(00)70017-X
17. Cao J, Wang X, Mills FJ (2002) Characterization of Sheet Buckling Subjected to Controlled Boundary Constraints. ASME J. of Manufacturing Science and Engineering 124:493–501. https://doi.org/10.1115/1.1475990
18. Emmens WC, van den Boogaard AH (2009) Incremental forming by continuous bending under tension - an experimental investigation. J Mater Process Technol 209(14):5456–5463. https://doi.org/10.1016/j.jmatprotec.2009.04.023
19. Hadoush A, van den Boogaard AH, Emmens WC (2011) A numerical investigation of the continuous bending under tension test. J Mater Process Technol 211(12):1948–1956. https://doi.org/10.1016/j.jmatprotec.2011.06.013
20. Ai S, Dai R, Long H (2020) Investigating formability enhancement in double side incremental forming by developing a new test method of tension under cyclic bending and compression. J Mater Process Technol 275:116349. https://doi.org/10.1016/j.jmatprotec.2019.116349
21. Ai S, Long H (2022) Biaxial tension under bending and compression - development of a new formability test for incremental sheet forming. IOP Conference Series: Materials Science and Engineering 1270(1). https://iopscience.iop.org/article/10.1088/1757-899X/1270/1/012066
22. Paul SK (2021) Controlling factors of forming limit curve: a review. Adv Ind Manuf Eng 2:100033. https://doi.org/10.1016/j.aime.2021.100033
23. ISO 12004-2:2008 (2008) Determination of forming limit curves for sheet and in the laboratory. Edition 2, 2008. https://www.iso.org/standard/43621.html
24. ISO 12004-2:2021 (2021) Determination of forming limit curves for sheet and in the laboratory. Edition 2, 2021. https://www.iso.org/standard/78138.html
25. Shao Z et al (2018) Experimental investigation of forming limit curves and deformation features in warm forming of an aluminium alloy, Proc. Inst. Mech. Eng. Part B J Eng Manuf 232(3):465–474. https://doi.org/10.1177/095440541664
26. Marciniak Z, Kuczyński K (1967) Limit strains in the processes of stretch-forming sheet metal. Int J Mech Sci 9(9):609–620. https://doi.org/10.1016/0020-7403(67)90066-5
27. Hosford WF, Duncan JL (1999) Sheet metal forming: a review. JOM 51(11):39–44. https://doi.org/10.1007/s11837-999-0221-5
28. Schreyer S, Volk W (2016) Optimization of the Modified Yoshida Buckling Test to Investigate the Influence of Curvature, Advanced Materials Research, 1140(2016): 67–74. https://www.scientific.net/AMR.1140.67
29. Emmens WC, van den Boogaard, Antonius H, van der Weijde DH (2009) The FLC, enhanced formability, and incremental sheet forming. International Deep Drawing Research Group annual conference, Golden Colorado, pp 773–784. http://purl.org/utwente/69291